Insight into Electronic, Optoelectronic and Thermoelectric Properties of Full-Heusler X_2 TaSi (X = Rb, K): First-Principles Calculations

N. SAIDI*, W. BENSTAALI, A. ABBAD, H. BENTAHAR AND S. BENTATA

Laboratory of Technology and Solid Properties, Abdelhamid Ibn Badis University, Mostaganem, Algeria

Received: 26.05.2025 & Accepted: 15.09.2025

Doi: 10.12693/APhysPolA.148.136 *e-mail: saidi.noureddine.etu@univ-mosta.dz

In this study, we have examined structural, electronic, magnetic, optic, thermoelectric, and elastic properties of full-Heusler alloys X₂TaSi (where X = Rb and K). First-principles calculations were performed to analyze the data, with the full-potential linearized augmented plane-wave method serving as the underlying basis. This method is firmly rooted in density functional theory. The calculations were executed using the WIEN2k code, firstly with the generalized gradient approximation and then with its modified Becke-Johnson version, which is commonly used to enhance the band gap values and align them with experimental findings, if available. The results related to the electronic and magnetic properties indicate that the full-Heusler alloys X₂TaSi (where X = Rb and K) exhibit half-metallic ferromagnetic behavior. Optical results demonstrated that the Heusler compounds K₂TaSi and Rb₂TaSi exhibit strong absorption and reflectivity in the ultraviolet range. These findings suggest that these compounds have significant potential for utilization in optical and optoelectronic devices within this spectrum. The findings of thermoelectric properties indicate that the X_2 TaSi alloys (where X = Rband K) are N-type semiconductors, as evidenced by their negative Seebeck coefficients. These alloys also exhibit high ZT values close to unity at low and medium temperatures. The elastic properties of the Rb₂TaSi compound suggest that it is mechanically stable and relatively ductile. In contrast, the K₂TaSi compound exhibits a relatively brittle nature.

topics: half-metallic ferromagnetics (HMFs), density functional theory (DFT), optical properties, modified Becke-Johnson-generalized gradient approximation (mBJ-GGA)

1. Introduction

Since their discovery in 1903 by Friedrich Heusler, Heusler alloys have been of interest. It has been reported that ferromagnetic alloys can be made from non-ferromagnetic constituents [1]. These ternary alloys are of the form X_2YZ , where Y and X are typically transition metals and Z is a main group element with s or p valence electrons (e.g., Al, In, Sb, Si, Ge, or Sn). Most of these alloys have an L2₁ crystal structure with a face-centered cubic (fcc) lattice [2].

Additional research revealed a connection between the magnetic properties of these alloys and their chemical composition (L2₁ structure), as well as the arrangement of Y atoms on an fcc sublattice [3]. Recently, half-metallic ferromagnetics (HMFs) have garnered significant attention due to their demonstrated potential for spintronics, as evidenced by their tunneling magnetoresistance (TMR) and giant magnetoresistance (GMR) properties [4]. Additionally, these materials have

applications in electromechanical systems [5]. Subsequent to the seminal work of de Groot et al. [6], a substantial body of additional materials has been obtained both theoretically and experimentally, thereby enabling the exploration of HMF properties. With the exception of Heusler and half-Heusler alloys [6], the subject of half-metallic behavior is addressed. The presence of the element (transition metals such as Fe, Ta, or Mn) has been identified in the perovskite structure [7], as well as in dilute magnetic materials. Semiconductors [8], certain oxides [9], and materials exhibiting a zinc-blend structure [10, 11] are of particular interest. A significant proportion of Heusler alloys of the X₂YZ stoichiometric composition are deemed suitable candidates for devices based on spin injection, such as the GMR and the substantial TMR in magnetoelectronic devices.

Additionally, they have the capacity to function as impeccable spin filters and spin injection devices, thereby serving as a substitute for ferromagnetic 3d metals. In this study, we focus on two compounds that have not been explored in the scientific

literature yet, namely K₂TaSi and Rb₂TaSi. For the first time, a comprehensive theoretical analysis based on first-principles quantum mechanical calculations is conducted to investigate a range of fundamental physical properties, including structural stability, electronic structure, magnetic properties, elastic properties, optical behavior, and thermoelectric performance. These compounds were selected because they have not yet attracted attention in theoretical or experimental research, which highlights the novelty and significance of this work. This study aims to provide a solid theoretical foundation to support future experimental synthesis efforts and to assess their potential applicability in spintronic devices, magneto-electronic systems, and energy conversion technologies.

2. Method of calculation

Density functional theory (DFT) [12] is a systematic approach for evaluating the ground-state description of a material and gaining an in-depth understanding of its physical properties. A rigorous and precise determination of the ground-state parameters for X_2 TaSi materials (where X = Rb, K) has been achieved through the implementation of DFT within the framework of the Full-Potential Linearized Augmented Plane Wave (FP-LAPW) method, as facilitated by the WIEN2k software package [13, 14]. The Perdew-Burke-Ernzerhof (PBE-GGA) scheme within the generalized gradient approximation (GGA) was utilized to calculate the exchange-correlation functional, thereby accounting for the strong on-site correlation of the 3d electrons. However, the band structure at the optimized lattice constants was calculated using the modified Becke-Johnson (TB-mBJ) exchange-correlation potential proposed by Tran and Blaha [15], which is known for its ability to provide improved estimates of band gap values.

In the context of the plane wave expansion, a cutoff parameter of $R_{\rm mt}$ $K_{\rm max}=8$ was employed, where $R_{\rm mt}$ denotes the smallest atomic sphere radius (RMT), and K_{max} signifies the maximum wave vector in the interstitial region. To achieve superior convergence in the self-consistent calculations, a k-mesh of 4000 points was utilized. This value was selected after a thorough convergence test (Fig. 1), where the total energy was evaluated for increasingly dense grids, and the final choice corresponded to the point at which the variation in energy per atom was less than 0.1 meV, ensuring reliable self-consistent field (SCF) calculations. The total charge for the current set of alloys was set to 10^{-4} electrons. Furthermore, the elastic and optical package [16] was integrated into the computations. Using the WIEN2k simulation code, the elastic constants and optical properties were calculated, providing valuable insights into

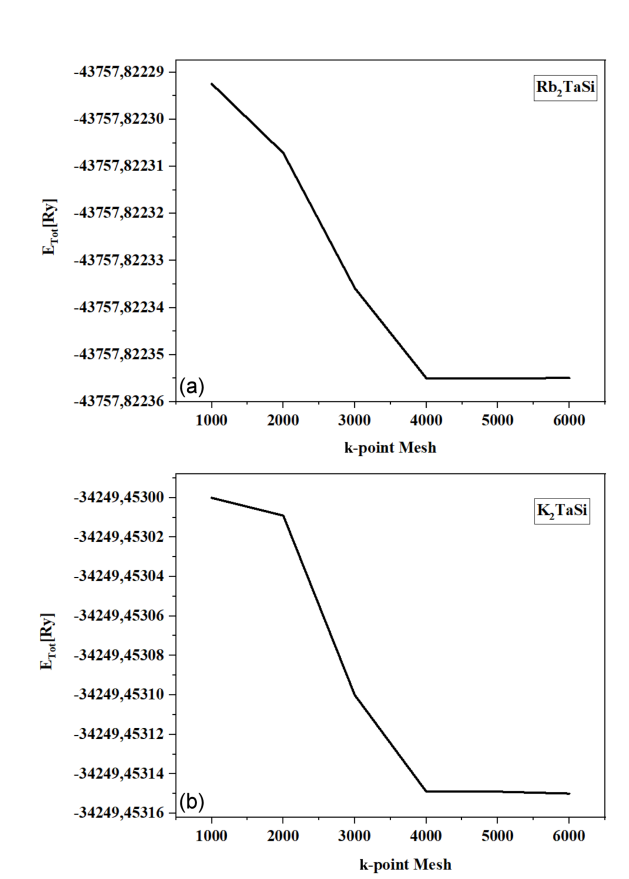


Fig. 1. Convergence test for self-consistent field (SCF) calculations for (a) Rb₂TaSi and (b) K₂TaSi.

the mechanical stability and electronic structure of the material. The transport properties of the compounds were calculated using the BoltzTraP code [17].

3. Results and discussion

The predicted properties of the studied alloys have been classified into separate sections, with each section addressing a specific property that was analyzed. These properties have been organized under superordinate headings that accurately reflect the content of each respective section.

3.1. Structural and elastic properties

3.1.1. Structural properties

Predicting the crystal structure of materials is a fundamental step in computational material discovery, as it enables visualization of the microscopic geometry of the material and provides insights into the relative stability of different structures and the possibility of transitions between

TABLE I Optimized lattice constant (a_0) , bulk modulus (B_0) , and its pressure derivative (B'), formation energy (ΔH_f) of X_2 TaSi (X = Rb, K).

Material	a_0 [Å]	Volume $[(u.a)^3]$	B [GPa]	B'	ΔH_f	Energy [Ry]
K_2TaSi	7.4146	687.6949	30.8812	4.2317	-0.4615	-34240.453143
Rb ₂ TaSi	7.7139	774.3963	26.5993	4.7036	-0.3810	-43757.822368

them [18]. In this section, we focused on studying the structural properties of our X₂TaSi alloys (where X = Rb and K) for two types of crystal structures, namely Hg₂CuTi and Cu₂MnAl, and in three magnetic states: ferromagnetic (FM), nonmagnetic (NM), and antiferromagnetic (AFM). Results of energy optimization (using 1500k mesh points) show that these alloys are stable in the FM state, as shown in Fig. 2. According to this figure, the preferred crystal structure for this study is Hg₂CuTi (FM), because this particular structure corresponds to the most energetically favorable configuration, yielding the lowest total energy of all possibilities considered. The atoms occupy the following crystallographic positions given according to Wyckoff notation: X-I at coordinates (0,0,0), X-II at (1/4, 1/4, 1/4) (either Rb or K), the element Ta at (1/2, 1/2, 1/2), and Si at (3/4, 3/4, 3/4). These atomic arrangements confirm that the compounds crystallize in the full-Heusler structure of the $L2_1$ type, which belongs to the cubic system with space group F-43m (no. 216) [19]. This is due to the fact that the given atomic positions indicate that: (i) there are two equivalent X atoms on the 8c sites, (ii) the transition metal (Ta) is at 4a, and (iii) the main group element (Si) is at 4b. The atomic coordinates reproduce the Wyckoff site occupancy pattern of the L2₁ type, which is what defines this structure crystallographically. Such a Wyckoff site occupation represents the characteristic signature of the L2₁ full-Heusler structure, thereby confirming that the compounds studied crystallize in this prototype. The calculated ground-state properties are summarized in Table I, which includes the lattice constant (a_0) , the minimum volume (V_0) , the bulk modulus (B_0) , and the pressure derivative of the bulk modulus (B_n) . To evaluate the structural stability of these alloys, we accurately calculated the ground-state properties using Murnaghan's equation [20], which is given by

$$E(V) = E_0 + \frac{B_0}{B_0'(B_0'-1)} \left[V \left(\frac{V_0}{V} \right)^{B_0'} - V_0 \right] + \frac{B_0}{B_0'} (V - V_0).$$
(1)

In addition to calculating the lattice constants, the formation energy was also computed to evaluate the thermodynamic stability of the studied compounds. The formation energy ΔH_f serves as a key

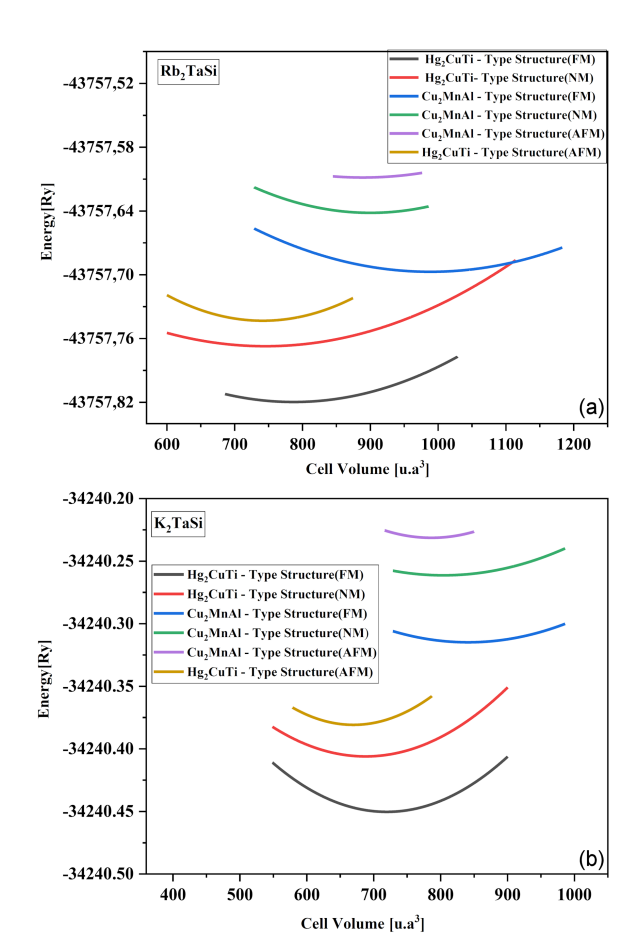


Fig. 2. Energy-volume optimization curves for (a) Rb₂TaSi and (b) K_2 TaSi Heusler alloys computed for two different structural types (Hg_2CuTi , Cu_2MnAl) and three different phases (ferromagnetic (FM), antiferromagnetic (AFM), and non-magnetic (NM)).

indicator for predicting the experimental feasibility of synthesizing the material and is determined using the following relation [21]

$$\Delta H_f = E_{\text{formation}}^{\text{X}_2\text{TaSi}} = E_{\text{total}}^{\text{X}_2\text{TaSi}} - \left(2E_{\text{bulk}}^{\text{X}_2} + E_{\text{bulk}}^{\text{Ta}} + E_{\text{bulk}}^{\text{Si}}\right). \tag{2}$$

In (2), $E_{\rm total}^{\rm X_2 TaSi}$ is the total energy of the full-Heusler structure, and $E_{\rm bulk}^{\rm X_2}$, $E_{\rm bulk}^{\rm Ta}$, and $E_{\rm bulk}^{\rm Si}$ represent the energies of the individual elements X, Y, and Z, respectively. If ΔH_f is negative ($\Delta H_f < 0$), it

indicates that the compound is stable. If ΔH_f is positive $(\Delta H_f > 0)$, it suggests that the compound is unstable [22].

The calculated formation energies for the compounds are as follows

$$\Delta H_f(\text{Rb}_2\text{TaSi}) = -0.3810 \text{ eV},$$

$$\Delta H_f(K_2 \text{TaSi}) = -0.4615 \text{ eV}. \tag{3}$$

The negative values of the formation energy indicate that both compounds possess thermodynamic stability, meaning they are energetically favorable and can be synthesized experimentally. Moreover, the more negative value for K_2 TaSi suggests that it is slightly more stable than Rb_2 TaSi.

3.1.2. Elastic properties

In the field of physics, elasticity is defined as a fundamental property of materials. It offers significant information about the stability, ductility, and rigidity of a material subjected to external forces that may cause alterations in its shape or volume. In the context of cubic crystals, three primary independent elastic constants are identified: C_{11} , C_{12} , and C_{44} [23]. In order to analyze the elastic behavior of our compounds, it is essential to calculate the elastic constants C_{ij} and related physical properties. In addition, these constants must satisfy the mechanical stability criteria that are specific to cubic crystals [24–26]. Therefore,

$$C_{11} > C_{12}, \quad C_{44} > 0, \quad C_{11} > 0,$$
 (4)

$$C_{11} > B > C_{12},$$
 (5)

$$C_{11} + 2C_{12} > 0. (6)$$

Furthermore, a multitude of additional mechanical properties can be derived from the calculated elastic constants, including bulk modulus B, shear modulus G, Young's modulus \mathcal{E} , Poisson's ratio ν , and the anisotropy factor A (see Table II). These are obtained using the Voigt–Reuss–Hill approximation [27, 28], based on the following relations

$$B = \frac{C_{11} + 2C_{12}}{3},\tag{7}$$

$$V = \frac{3B - 2G}{2(3B + G)},\tag{8}$$

$$A = \frac{2C_{44}}{C_{11} - C_{12}},\tag{9}$$

$$\mathcal{E} = \frac{9BG}{3B+G},\tag{10}$$

$$G = \frac{2C_{44}}{C_{11} - C_{12}}. (11)$$

In fact, B, G, and \mathcal{E} are used to characterize materials in terms of their compressibility and rigidity. The bulk modulus B is indicative of the material's resistance to volume change under pressure, while

TABLE II

Elastic constants C_{ij} [GPa], bulk modulus B [GPa], shear modulus G [GPa], Pugh's ratio B/G, Young's modulus \mathcal{E} [GPa], Poisson's ratio ν , and anisotropy factor A calculated at the equilibrium volume for full-Heusler X₂TaSi (X = Rb and K) alloys.

Parameters	Unit	Alloys				
	Onic	Rb_2TaSi	$ m K_2TaSi$			
C_{11}		51.765	55.052			
C_{12}		14.344	19.123			
C_{44}		15.826	20.166			
B	[GPa]	26.817	31.099			
G	[GPa]	16.928	19.248			
B/G		1.584	1.615			
E	[GPa]	41.960	47.870			
A		0.845	1.122			

the shear modulus G signifies its capacity to resist plastic deformation. The ratio B/G serves as a critical indicator for describing the plastic behavior of materials. The mechanical analysis of the Rb₂TaSi and K₂TaSi compounds reveals a clear difference in their elastic properties, reflecting the influence of chemical composition on their behavior under mechanical stress. The K₂TaSi compound demonstrates relatively enhanced mechanical characteristics, indicated by higher elastic constants such as $C_{11} = 55.052$ GPa and $C_{44} = 20.166$ GPa, along with a bulk modulus of B = 31.099 GPa and Young's modulus $\mathcal{E} = 47.870$ GPa, signifying greater resistance to compression and deformation. Additionally, its shear modulus $G \approx 19.248$ GPa is higher than that of Rb₂TaSi, confirming better mechanical stiffness.

The B/G ratio of 1.615 and Poisson's ratio $\nu \approx 0.243$ suggest that K_2 TaSi possesses a moderate level of ductility, which is a desirable trait for various industrial applications. On the other hand, although Rb_2 TaSi exhibits lower values for most mechanical parameters (B=26.817 GPa and $\mathcal{E}=41.960$ GPa), it still falls within the acceptable range of mechanical stability and shows similar ductility characteristics, with a B/G ratio of 1.584 and Poisson's ratio $\nu \approx 0.239$. Based on these results, both compounds can be classified as mechanically stable, with K_2 TaSi showing a slight advantage in stress resistance, making it a more suitable candidate for applications requiring a balanced combination of stiffness and ductility.

3.2. Electronic properties

The study of band structure and density of states (DOS) is fundamental for understanding the electronic, optical, and magnetic properties of

TABLE III Electronic band gap characteristics of X_2 TaSi (X = Rb, K) Heusler alloys under GGA and mBJ-GGA method.

Compounds	GGA		$\mathrm{mBJ} ext{-}\mathrm{GGA}$		Nature of	Band gap type
Compounds	spin up	spin down	spin up	spin down	the compounds	(mBJ-GGA)
Rb_2TaSi	metallic	0.6 eV	metallic	1.25 eV	half metallic	direct
K_2TaSi	${ m metallic}$	$_{ m metallic}$	metallic	1.57 eV	half metallic	direct

materials. The band structure reveals the allowed energy levels and dispersion of electrons, while DOS provides information on the number of available electronic states at each energy level. These insights are crucial for predicting material behavior in semiconductors, metals, and spintronic applications. Accurate knowledge of these properties enables the design of materials with tailored functionalities. Moreover, they are essential for interpreting experimental results from techniques such as angle-resolved photoemission spectroscopy (ARPES) or X-ray photoelectron spectroscopy (XPS).

3.2.1. Band structure

In this section, the electronic structures of the full-Heusler alloys X_2 TaSi (X = Rb and K) are discussed. Figure 3 illustrates the band structures along the high-symmetry points of the Brillouin zone [29], which have been calculated using the Perdew-Burke-Ernzerhof (PBE-GGA) and the modified Becke-Johnson method within the generalized gradient approximation (mBJ-GGA). The GGA results for the compound Rb₂TaSi show an energy gap of about 0.6 eV in the spin-down channel (Fig. 3b), indicating semiconducting behavior in this state. In contrast, the compound exhibits metallic behavior in the spin-up channel (Fig. 3e), where the valence band maximum (VBM) lies along the L- Γ direction at an energy ≈ 0.015 eV above the Fermi level. Based on this clear difference in electronic behavior between the two spin channels, the Rb₂TaSi compound can be classified as a halfmetallic material, as shown in Table III. For the compound K₂TaSi (Fig. 3c, d), the calculations show a clear metallic behavior in both spin channels, reflecting a fully metallic nature for this compound. In the spin-down channel, the conduction band minimum (CBM) lies along the X direction at an energy of ≈ -0.023 eV below the Fermi level. In the spin-up channel, the valence band maximum (VBM) lies along the L–Γ direction at an energy estimated to be 0.013 eV above the Fermi level.

On the other hand, when using the mBJ-GGA method (see Fig. 3e-h), we found that K₂TaSi compound has a relatively larger energy gap of 1.57 eV in the spin-down channel, while for the Rb₂TaSi compound it reaches 1.25 eV. It is worth noting that both compounds exhibit a direct band gap

along the X direction. For the spin-up channel (Fig. 3e, g), both compounds have metallic behavior as confirmed in Fig. 4 by the density of states (DOS). Based on these results, we found that the compounds K_2 TaSi and Rb_2 TaSi exhibit halfmetallic behavior. Obtained results for both compounds when using mBJ-GGA revealed a clear difference in the electronic behavior between the two spin channels of each compound since the down channel shows semiconducting behavior and the up channel shows metallic behavior.

3.2.2. Density of states

In Fig. 4, density of states (DOS) plots for the material system are presented. The results have been obtained using two different exchange—correlation functionals, namely generalized gradient approximation (GGA) and the modified Becke—Johnson generalized gradient approximation (mBJ-GGA). These plots are essential tools for understanding the electronic structure of the material, particularly the energy gap, orbital contributions, and spin polarization.

In the case of using GGA (see Fig. 4), the total density of states (TDOS) reveals a clear energy gap of ≈ 0.6 eV in the spin-down channel, indicating semiconducting behavior, while the spinup channel exhibits metallic behavior, suggesting that the Rb₂TaSi compound has a half-metallic nature. As for the K₂TaSi compound, it shows a metallic nature in both spin channels (spin-up and spin-down), confirming its overall metallic character within GGA. According to mBJ-GGA, both Rb₂TaSi and K₂TaSi compounds exhibit clear halfmetallic behavior — the spin-up channel remains metallic, while the spin-down channel displays semiconducting characteristics, with an energy gap estimated to be ≈ 1.57 eV for K₂TaSi and 1.25 eV for Rb₂TaSi. This observation is further supported by band structure analysis.

Moreover, the density of states enables the identification of the electronic contributions from each individual atom and each type of orbital (s, p, d), offering a deeper understanding of the origin of the compound's electronic behavior, as discussed below.

The individual orbital contributions indicate a significant role of $\operatorname{Ta-}d$ orbitals near the Fermi level, along with a notable contribution from $\operatorname{Si-}p$ orbitals

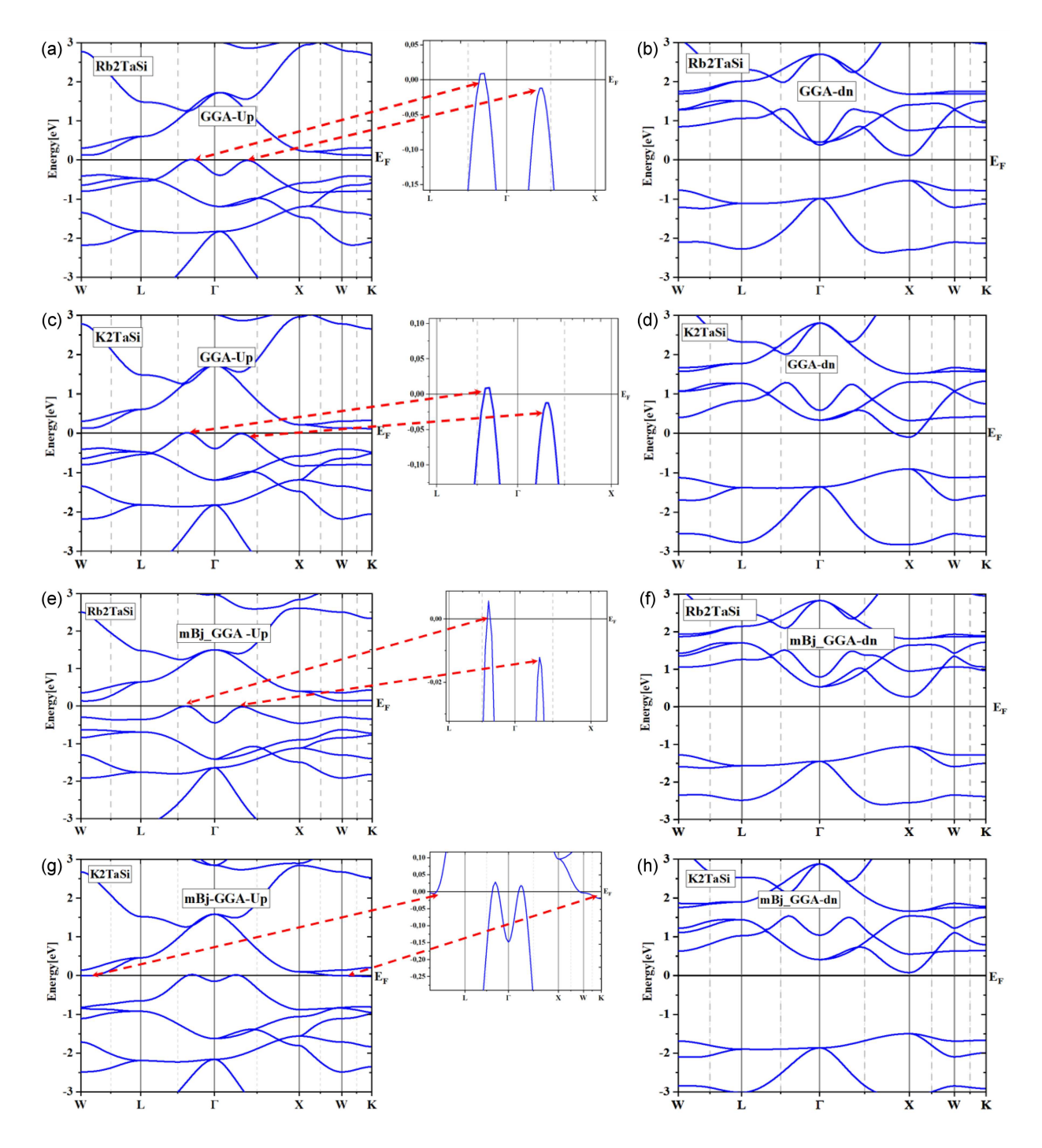


Fig. 3. The band structure of the full-Heusler alloys X_2 TaSi (X = Rb and K) was calculated using (a-d) the GGA and (e-h) mBJ-GGA methods within the ferromagnetic (FM) configuration.

to the electronic structure. When using mBJ-GGA (Fig. 4), the overall shape of the DOS remains similar to that obtained with GGA; however, the energy gap appears slightly larger. This suggests that mBJ-GGA provides a more accurate treatment of exchange interactions.

The Ta-d orbitals continue to dominate near the Fermi level, with observable shifts in peak positions and intensities compared to the GGA results. A detailed examination of the orbital-resolved DOS

(Fig. 4) confirms that Ta-d orbitals are highly active near the Fermi level, contributing substantially to both the valence and conduction bands. This underscores the critical role of Ta in defining the material's electronic properties, such as conductivity and potential magnetic behavior. The Si-p orbitals are mainly involved in the valence band, affecting the material's optical and electrical responses. In contrast, the contributions of Rb and K are very small for the two approximations (GGA and

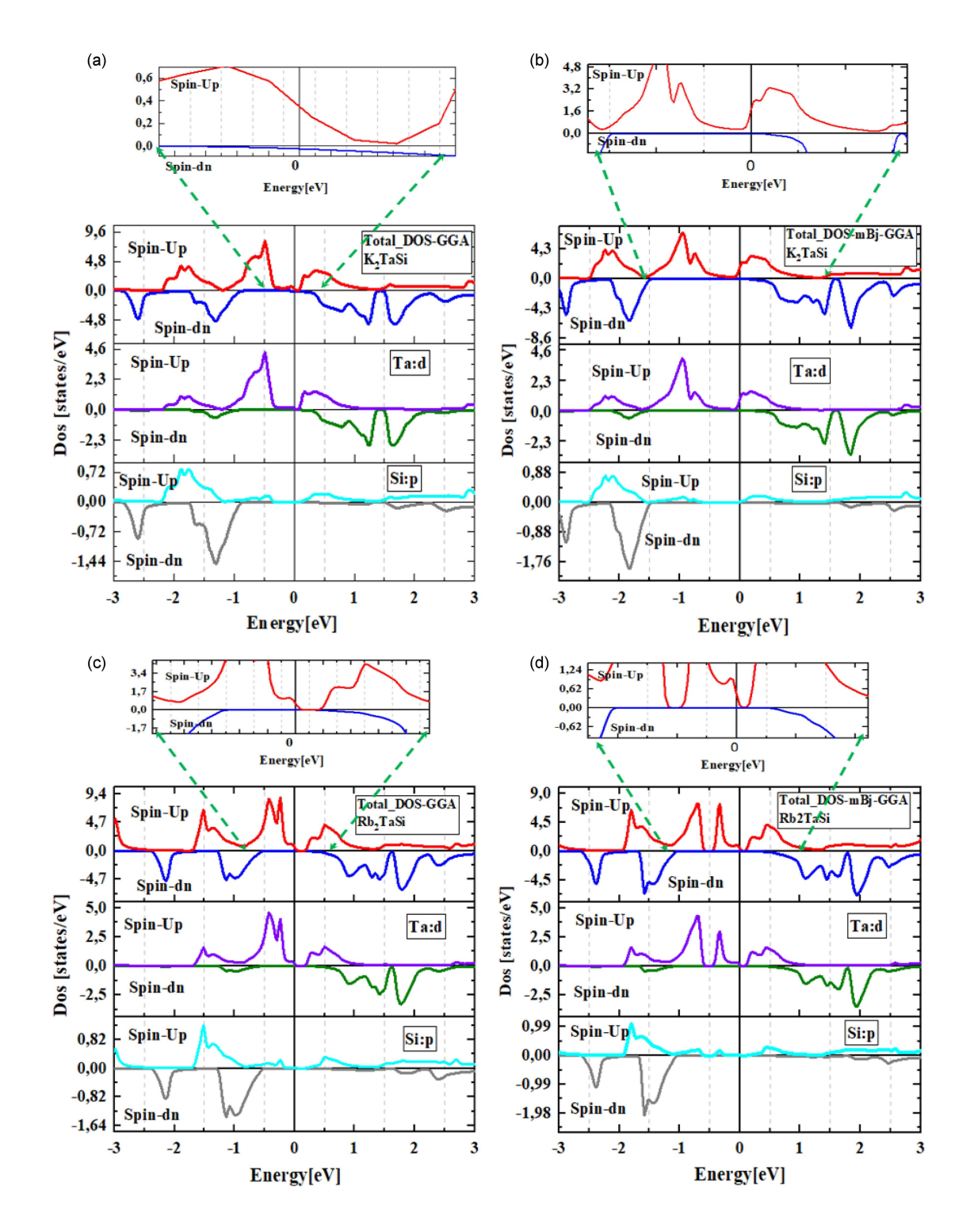


Fig. 4. (a-d) TDOS and partial density of states (PDOS) for the full-Heusler X_2 TaSi (X = Rb and K) alloys, using mBJ-GGA.

mBJ-GGA); these low values have no influence on the interactions between components. Overall, while the general trends in orbital contributions are consistent across both GGA and mBJ-GGA functionals, the latter approximation yields a more precise depiction of the electronic structure, especially in terms of the energy gap and the characteristics of Ta-d orbital peaks.

3.3. Magnetic properties

The magnetic properties (μ) of the K_2TaSi and Rb_2TaSi alloys reveal several notable trends that are influenced by both the elemental contributions and the choice of computational method. The mBJ-GGA potential generally enhances

TABLE IV

The calculated total (μ^{tot}) and partial $(\mu^{X1}, \mu^{X2}, \mu^{Ta}, \mu^{Si}, \mu^{int})$ magnetic moments $[\mu_B]$ for the full-Heusler X_2 TaSi alloys (X = Rb and K) were obtained using GGA and mBJ-GGA; here, μ^{X1} and μ^{X2} are the magnetic moments of the first and the second X atom (X = Rb and K) in the alloy, respectively, and μ^{Ta} , μ^{Si} , and μ^{int} are the magnetic moments of Ta, Si, and interstitial region, respectively (all magnetic moments are given in Bohr magnetons).

A 11	3.6 (1 1	. X1	X2	. Ta	μ^{Si}	int	tot
Alloys	Method	μ^{m}	μ^{12}	μ^{ra}	μ°	μ^{cos}	μ^{tot}
$ m K_2TaSi$	GGA	0.038	0.086	1.860	-0.182	1.200	3.002
	mBj-GGA	0.036	0.082	1.973	-0.289	1.197	3.000
$\mathrm{Rb_2TaSi}$	GGA	0.033	0.064	1.913	-0.208	1.203	3.005
	mBi-GGA	0.028	0.058	2.035	-0.289	1.188	3.000

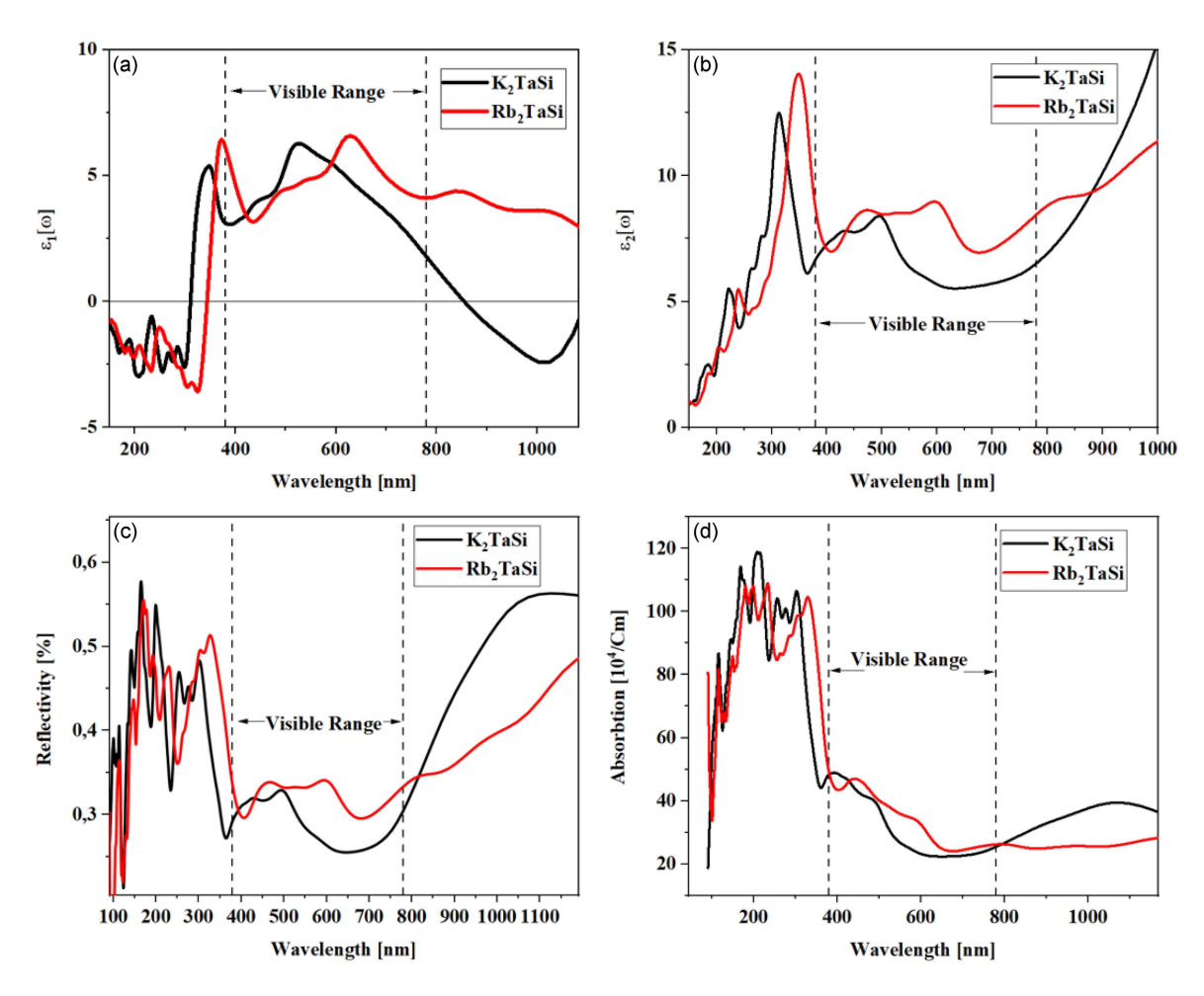


Fig. 5. Variation of optical and dielectric properties of X_2 TaSi (X = Rb, K) Heusler alloys as functions of wavelength: (a) real part and (b) imaginary part of the dielectric constant in spin-down channels, (c) reflectivity index, (d) absorption coefficient.

the magnetic moments of tantalum (Ta) while reducing those of potassium (K) and rubidium (Rb) compared to the GGA potential. Additionally, mBJ-GGA increases the negative magnetic moment of silicon (Si), indicating stronger antiferromagnetic coupling. Among the elements, Ta plays a dominant role in determining the magnetic behavior due to its substantial positive value of μ , whereas

Si contributes negatively through antiferromagnetic interaction. The magnetic moments of Rb and K are relatively small, suggesting weaker spin polarization. Both K₂TaSi and Rb₂TaSi alloys exhibit a total magnetic moment close to 3.0 $\mu_{\rm B}$, reflecting near-saturation of magnetization, with consistent results across both computational approaches, underscoring their reliability as shown in Table IV.

These magnetic properties demonstrate the great potential of full-Heusler compounds in a wide range of technological applications. Among the most promising uses are computer memory devices, spintronic technology, magnetic sensors, transformer cores, and microwave components [30]. These applications benefit from artificial ferrimagnetic elements to enable magnetic polarization control, making these materials strong candidates for the development of advanced magnetic technologies in the future [31–34].

3.4. Optical properties

The optical properties of K_2 TaSi and Rb_2 TaSi were investigated in order to capitalize on their electronic features for semiconductor applications. The optical properties reveal information about the material's interaction with light and its ability to absorb, reflect, and transmit electromagnetic radiation. We can gain significant insight into their behavior at various wavelengths and their possible usage in optoelectronic devices. This part presents an investigation of the real component $(\varepsilon_1(\omega))$ and imaginary component $(\varepsilon_2(\omega))$ of the dielectric function, as well as the absorption coefficient $(\alpha(\omega))$ and reflectivity $(R(\omega))$ [35].

One of the most significant optical properties is the dielectric function, which describes the reaction of a material to an electromagnetic field. Its real part ε_1 describes the disappearance of electromagnetic waves (Fig. 5a); this usually refers to the case when the wave is absorbed as it passes through the material. Note that ε_1 is also inversely associated with the gap energy. We found that K_2 TaSi shows metallic behavior in the range from 100 to 315 nm (12.4 to 3.93 eV), and Rb₂TaSi from 100 to 350 nm (12.4 to 3.54 eV). Outside these ranges, both compounds behave like dielectrics.

In Figure 5b, the imaginary part of the dielectric function, $\varepsilon_2(\omega)$, shows the transitions between occupied and unoccupied states in the valence and conduction bands [36]. The drop in $\varepsilon_2(\omega)$ at near 400 nm (3.09 eV) reflects a slowdown in absorption, which we can clearly notice in Fig. 5d. For both compounds, the main absorption is located in the UV region with a peak at 250 nm (4.96 eV), followed by a sharp drop to a value of 45×10^4 (C m)⁻¹ at a wavelength of 400 nm (3.09 eV). In fact, the compounds K_2 TaSi and Rb_2 TaSi exhibit a small amount of visible light absorption. As a result, they are suitable for device applications in the UV region of the spectrum.

The reflectance spectrum in Fig. 5c illustrates the amount of incident light reflected by a material, which is influenced by the surface roughness, refractive index, and electronic band structure of the material. Both materials tested exhibit maximum

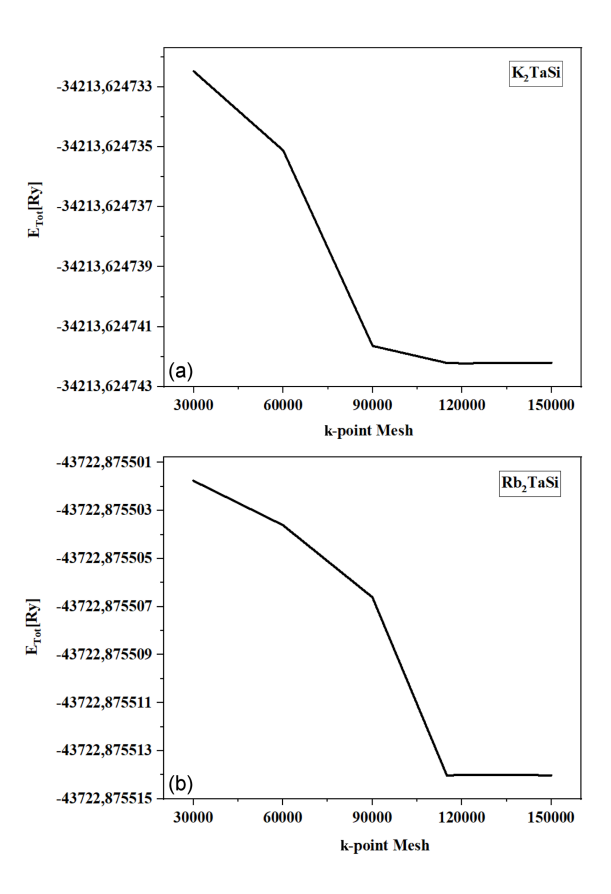


Fig. 6. Convergence test for thermoelectric properties for (a) K₂TaSi and (b) Rb₂TaSi.

reflectivity in the range from 100 to 350 nm (12.4 to 3.54 eV), indicating a strong capacity for light reflection within this range. Now, by analyzing the main optical properties — dielectric function, absorption, and reflectivity — we can understand how electronic transitions occur in K_2 TaSi and Rb_2 TaSi. This information is useful in the design of photonics and optoelectronic devices.

It is worth mentioning that the conversion relationship between the photon energy E [eV] and the ultraviolet (UV) wavelength range has been thoroughly discussed in [37].

3.5. Thermoelectric properties

The conversion of heat flow into electrical energy, and vice versa, is achieved through thermoelectric materials [38–40]. The objective of this study is twofold: First, to contribute to the development of electricity production from residual (wasted) heat without greenhouse gas emissions, and second, to the development of refrigeration systems without cryogenic fluids [41]. To achieve this objective, further research is necessary to identify suitable thermoelectric materials. The primary challenge facing materials scientists concerns the enhancement of

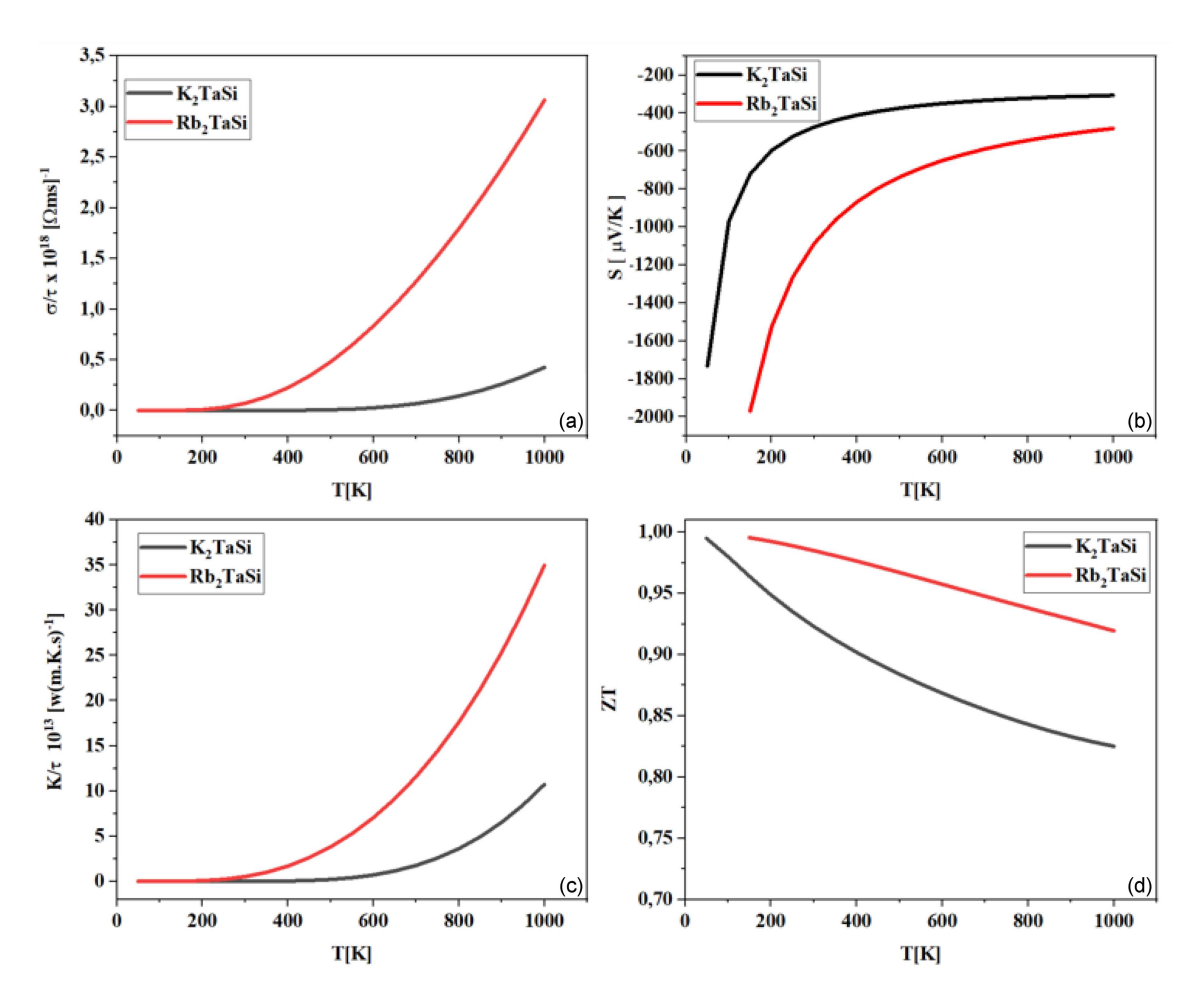


Fig. 7. Variation of the thermal and electrical properties of X_2 TaSi Heusler compounds (where X = Rb, K) as a function of temperature. These are: (a) electrical conductivity (σ/τ) , (b) Seebeck coefficient (S), (c) thermal conductivity (κ/τ) , (d) figure of merit (ZT).

the performance of thermoelectric materials. The performance of these materials is quantified by the dimensionless figure of merit $ZT = ((S^2 \sigma T)/K)$, where S, σ , T, and K represent the Seebeck coefficient, electrical conductivity, temperature, and total thermal conductivity, respectively.

To investigate the transport properties of full-Heusler alloys (X = Rb, K), the BoltzTraP code was employed in conjunction with the WIEN2k package. We have used 120000k points obtained after the convergence test (Fig. 6) to guarantee the numerical stability and accuracy of the transport calculations. In our study, the electrical conductivity is presented in the form of a ratio to the relaxation time (σ/τ) over the temperature range from 50 to 1000 K.

3.5.1. Electrical conductivity (σ/τ)

In Fig. 7a, the analysis of the behavior of electrical conductivity divided by relaxation time (σ/τ) for two materials, i.e., K_2TaSi and Rb_2TaSi , in a temperature range from 50 to 1000 K is presented.

At low temperatures (50–200 K), both materials exhibit stable values of σ/τ , indicating that the electrical conductivity is not significantly temperature-dependent in this temperature range. This phenomenon can be attributed to the limited charge carrier mobility.

Beginning at 200 K, the magnitude of the electrical resistivity, σ , begins to increase noticeably. In the case of Rb₂TaSi, the ratio σ/τ shows a clear exponential pattern, while in the case of K₂TaSi, the ratio shows a gradual increase in electrical conductivity. This observation indicates a tendency for Rb₂TaSi to exhibit semiconductor-like characteristics, in contrast to the metallic behavior exhibited by K₂TaSi.

At 1000 K, σ/τ reaches approximately $3.5 \times 10^{18} \ (\Omega \ m \ s)^{-1}$ for Rb₂TaSi, whereas it is equal to $\simeq 2.5 \times 10^{18} \ (\Omega \ m \ s)^{-1}$ for K₂TaSi. This reflects the high electrical conductivity at elevated temperatures, especially for Rb₂TaSi.

These disparities are ascribed to the electronic and structural properties of the constituent elements in each material, which influence the density and mobility of charge carriers.

3.5.2. Seebeck coefficient (S)

Figure 7b presents an analysis of the behavior of the Seebeck coefficient $(S [\mu V/K])$ as a function of temperature (T [K]). The two curves corresponding to the two compounds demonstrate analogous behavior, characterized by a swift rise in the Seebeck coefficient at low temperatures, followed by a gradual stabilization at higher temperatures. The Seebeck coefficient, which is a measure of the electrical resistance of a material when it is heated, is negative for both tested materials. This indicates that electrons are the dominant charge carriers in these materials, which is in contrast to p-type semiconductors, where holes dominate. At low temperatures (0 to 200 K), the absolute values of S are elevated, reaching around $-2000 \,\mu\text{V/K}$. Subsequently, as with increasing temperature, S undergoes a precipitous decline, attributable to the sequential activation of charge carriers. In the temperature range 200–600 K, the Seebeck coefficient S demonstrates a consistent increase, albeit at a reduced rate. Notably, Rb₂TaSi exhibits superior performance compared to K₂TaSi. As the temperature increases from 600 to 1000 K, the S values gradually level off and become nearly constant. Rb₂TaSi reaches approximately $-450 \mu V/K$, and K_2 TaSi reaches approximately $-480 \,\mu\text{V/K}$. This observation indicates that the thermoelectric transport mechanisms in these compounds attain a quasi-stable state at elevated temperatures.

In summary, $\mathrm{Rb_2TaSi}$ exhibits a higher absolute Seebeck coefficient compared to $\mathrm{K_2TaSi}$ across the entire temperature range, with a more significant disparity observed at low temperatures. These disparities can be ascribed to variations in the crystal structure or electronic properties caused by the different cations (Rb, K). The findings suggest that both materials demonstrate considerable thermoelectric potential, with $\mathrm{Rb_2TaSi}$ exhibiting marginally superior performance.

3.5.3. Thermal conductivity

Thermal conductivity (κ/τ) is a property of a material that quantifies its capacity for heat conduction, and it is a critical parameter in the assessment of thermoelectric performance [42]. This importance becomes evident when analyzing the temperature dependence of thermal conductivity. In Fig. 7c, it is shown how the thermal conductivity (k/τ) changes with temperature T [K] for two different materials. At low temperatures (0 to 200 K), the κ/τ values for both materials remain very low. This phenomenon can be attributed to limited phonon vibrations and a low number of active charge carriers. As a result of this phenomenon, the ability of the crystal lattice to conduct heat is reduced. As the temperature

increases from 200 to 600 K, the k/τ curves exhibit a rapid increase; Rb₂TaSi displays a clear exponential growth, while K₂TaSi shows a more gradual increase. This phenomenon is attributed to the progressive activation of charge carriers and the simultaneous increase in phonon vibrations, which collectively enhance the overall thermal conductivity of the material. At elevated temperatures ranging from 600 to 1000 K, the $\mathrm{Rb}_2\mathrm{TaSi}$ curve exhibits an upward trend, surpassing 35×10^{13} W/(m K s) and 10×10^{13} W/(m K s) in the power spectrum. In contrast, the K₂TaSi curve maintains a lower level, registering approximately $10 \times 10^{13} \; \mathrm{W/(m \; K \; s)}$, and undergoes a progressive decrease. Rb₂TaSi exhibits superior thermal conductivity to K₂TaSi across the entire temperature range studied, which is due to its electronic structure, which facilitates enhanced electron mobility. K₂TaSi, on the other hand, exhibits diminished thermal performance, which may be due to structural characteristics that impede heat transport. The findings indicate that both materials demonstrate an enhancement in thermal conductivity with an increase in temperature, albeit with varying degrees of dominance. At elevated temperatures, the electronic component becomes predominant, while the lattice contribution gradually decreases.

3.5.4. Figure of merit (ZT)

Figure 7d illustrates the evolution of the thermoelectric figure of merit (ZT) as a function of temperature for K₂TaSi and Rb₂TaSi; one can observe a gradual decrease in the ZT values with increasing temperature. At low temperatures (0-200 K), the ZT values are relatively high, with Rb₂TaSi slightly outperforming K₂TaSi due to a superior balance between electrical conductivity, Seebeck coefficient, and thermal conductivity. In the intermediate temperature range (200–600 K), ZT continues to decrease gradually, with Rb₂TaSi maintaining a slight advantage over K₂TaSi, reflecting better stability in the thermoelectric performance. At elevated temperatures ranging from 600 to 1000 K, the ZT values undergo a steady decrease. However, Rb₂TaSi consistently outperforms K₂TaSi, attaining a value of ≈ 0.92 as opposed to 0.85. This observation signifies that both materials retain their efficacy in hightemperature applications. The observed decline in ZT can be attributed to two phenomena, namely an increase in the lattice thermal conductivity and a relative decrease in the electronic conductivity and Seebeck coefficient with temperature. Notwithstanding this decline, the ZT values remain significant and promising — especially at higher temperatures — making both materials good candidates for thermoelectric applications, with Rb₂TaSi showing a slight overall advantage across the temperature range studied.

4. Conclusions

The structural, electronic, magnetic, elastic, optical, and thermoelectric properties of Heusler alloys X_2TaSi (where X=K and Rb) have been investigated using the WIEN2k package, which is a full-potential linearized augmented plane wave (FP-LAPW) method. The exchange–correlation energy was treated using both the generalized gradient approximation (GGA) and the modified Becke–Johnson potential (mBJ-GGA). Band structure calculations demonstrated that Rb_2TaSi and K_2TaSi are authentic half-metallic ferromagnets. These compounds exhibit magnetic moments of $3\mu_B$ per formula unit and possess direct band gaps of approximately 1.25 eV and 1.57 eV near the Fermi level in the minority spin channel, respectively.

The compounds K_2 TaSi and Rb_2 TaSi exhibit metallic behavior within specific wavelength ranges and act as insulators outside these ranges. These materials primarily absorb light in the ultraviolet region, exhibiting high reflectivity, which renders them suitable for a variety of optical and photonic applications. Therefore, these materials hold great promise for advanced optoelectronic devices that operate within the ultraviolet spectrum.

The thermoelectric properties of full-Heusler X_2 TaSi alloys were analyzed through a comprehensive study of the variation of the Seebeck coefficient S, electrical conductivity (σ/τ) , total thermal conductivity K, and figure of merit (ZT) as a function of temperature. The results indicate that these compounds behave as N-type semiconductors, as evidenced by their negative S across the entire studied temperature range. Furthermore, Rb₂TaSi and K_2 TaSi demonstrate notably high ZT values (calculated based on electronic contributions), particularly at low to medium temperatures, underscoring their considerable promise for thermoelectric applications.

Mechanical analysis shows that the compounds Rb₂TaSi and K₂TaSi exhibit mechanical stability, with K₂TaSi clearly superior in terms of stiffness and resistance to deformation. This is attributed to its higher values of elastic constants C_{ij} and Young's modulus \mathcal{E} . Overall, both compounds demonstrate good mechanical properties, making them suitable for use in fields that require durability and adequate mechanical resistance.

References

- [1] F. Heusler, Verh. Dtsch. Phys. Ges. 5, 219 (1903).
- [2] T. Graf, C. Felser, S.S.P. Parkin, *Prog. Solid State Chem.* 39, 1 (2011).
- [3] I. Galanakis, P.H. Dederichs, N. Papanikolaou, *Phys. Rev. B* **66**, 174429 (2002).

- [4] I. Žutić, J. Fabian, S. Das Sarma, Rev. Mod. Phys. 76, 323 (2004).
- [5] S.A. Wolf, D. Treger, *IEEE Trans. Magn.* **36**, 2748 (2000).
- [6] R.A. de Groot, F.M. Mueller, P.G. van Engen, K.H.J. Buschow, *Phys. Rev. Lett.* 50, 2024 (1983).
- [7] K.-I. Kobayashi, M.G. Kivelson, D.J. Stevenson, G. Schubert, C.T. Russell, R.J. Walker, C. Polanskey, *Nature* 395, 677 (1998).
- [8] K. Ono, J. Okabayashi, M. Mizuguchi, M. Oshima, A. Fujimori, H. Akinaga, J. Appl. Phys. 91, 8088 (2002).
- [9] K. Schwarz, J. Phys. F 16, L211 (1986).
- [10] W.-H. Xie, Y.-Q. Xu, B.-G. Liu, D.G. Pettifor, *Phys. Rev. Lett.* 91, 037204 (2003).
- [11] H. Shoren, F. Ikemoto, K. Yoshida, N. Tanaka, K. Motizuki, *Physica E* 10, 242 (2001).
- [12] E.S. Kryachko, E.V. Ludeña, *Phys. Rep.* **544**, 123 (2014).
- [13] W. Kohn, L.J. Sham, *Phys. Rev.* **140**, A1133 (1965).
- [14] P. Blaha, K. Schwarz, F. Tran,
 R. Laskowski, G.K.H. Madsen,
 L.D. Marks, J. Chem. Phys. 152, 074101 (2020).
- [15] F. Tran, P. Blaha, Phys. Rev. Lett. 102, 226401 (2009).
- [16] A. Otero-de-la-Roza, V. Luaña, Comput. Phys. Commun. 182, 1708 (2011).
- [17] G.K.H. Madsen, D.J. Singh, Comput. Phys. Commun. 175, 67 (2006).
- [18] A.R. Oganov, C.W. Glass, *J. Chem. Phys.* **124**, 244704 (2006).
- [19] A. Wederni, J. Daza, W.B. Mbarek, J. Saurina, L. Escoda, J.-J. Suñol, *Metals* 14, 688 (2024).
- [20] F.D. Murnaghan, Proc. Natl. Acad. Sci. USA 30, 244 (1944).
- [21] A.A. Emery, C. Wolverton, *Sci. Data* 4, 170153 (2017).
- [22] S. Berri, N. Bouarissa, *Acta Phys. Pol. A* **146**, 270 (2024).
- [23] G. Grimvall, *Thermophysical Properties of Materials*, Elsevier, Amsterdam 1999.
- [24] G.V. Sinko, N.A. Smirnov, J. Phys. Condens. Matter 14, 6989 (2002).
- [25] M. Born, K. Huang, Dynamical Theory and Experiment I, Springer, Berlin 1982.
- O. Beckstein, J.E. Klepeis, G.L. W. Hart,
 O. Pankratov, *Phys. Rev. B* 63, 134112 (2001).
- [27] W. Voigt, *Lehrbuch der Kristallphysik*, Teubner, Leipzig 1928.

- [28] A. Reuss, Z. Angew. Math. Mech. 9, 49 (1929).
- [29] O. Addou, A. Touia, K. Benyahia, Acta Phys. Pol. A 143, 252 (2023).
- [30] A.A. Yahaya, W.A. Yahya, A.S. Ahmed, A.A. Sholagberu, Acta Phys. Pol. A 145, 194 (2024).
- [31] A.B. Siad, M. Baira, F.Z. Dahou, K. Bettir, M.E. Monir, J. Solid State Chem. 302, 122362 (2021).
- [32] M.D.I. Bhuyan, S. Das, M.A. Basith, J. Alloys Compd. 878, 160389 (2021).
- [33] G.A.M. Mersal, H. Alkhaldi, G.M. Mustafa et al., J. Mater. Res. Technol. 18, 2831 (2022).
- [34] S. Haid, W. Benstaali, A. Abbad, B. Bouadjemi, S. Bentata, Z. Aziz, Mater. Sci. Eng. B 245, 68 (2019).
- [35] M. Fodil, O. Baraka, A. Mokadem, Acta Phys. Pol. A 146, 143 (2024).

- [36] S. Haid, B. Bouadjemi, K. Azil, T. Lantri, M. Houari, M. Matougui, S. Bentata, J. Electron. Mater. 53, 75 (2024).
- [37] V. Dalouji, *Heliyon* **10**, e37509 (2024).
- [38] G.S. Nolas, J. Poon, M. Kanatzidis, *MRS Bull.* **31**, 199 (2006).
- [39] T. Fang, S. Zheng, H. Chen, H. Cheng, L. Wanga, P, Zhang, RSC Adv. 6, 10507 (2016).
- [40] M. Matougui, B. Bouadjemi, M. Houari, S. Haid, T. Lantri, A. Zitouni, S. Bentata, B. Bouhafs, Z. Aziz, *Chin. J. Phys.* 57, 195 (2019).
- [41] C.L. Julian, *Phys. Rev.* **137**, A128 (1965).
- [42] L. Benahmedi, A. Besbes, R. Djelti, Acta Phys. Pol. A 147, 393 (2025).